Title

Efficient Atmospheric Cleansing of Oxidized Organic Trace Gases by Vegetation

Journal

Science, 330(6005)

ISSN

0036-8075

Authors

Karl, T

Harley, P

Emmons, L

et al.

Publication Date

2010-11-05

DOI

10.1126/science.1192534

Efficient atmospheric cleansing of oxidized organic trace gases by vegetation

T. Karl[1], P. Harley[1], L. Emmons[1], B. Thornton[2], A. Guenther[1],C. Basu[2], A. Turnipseed[1] and K. Jardine[3]

[1] National Center for Atmospheric Research, Boulder, CO, USA.
[2] School of Biological Sciences, University of Northern Colorado
Greeley, CO, USA
[3] Biosphere 2, University of Arizona, Tucson, AZ, USA.

The biosphere is the major source and sink of non methane volatile organic compounds (VOC) in the atmosphere. Gas phase chemical reactions initiate the removal of these compounds from the atmosphere, which ultimately proceeds via deposition at the surface or direct oxidation to CO or CO_2. We performed ecosystem scale flux measurements that show the removal of oxygenated VOC (oVOC) via dry deposition is substantially larger than currently assumed for deciduous ecosystems. Laboratory experiments indicate efficient enzymatic conversion and potential upregulation of various stress related genes leading to enhanced uptake rates as a response to ozone and methyl vinyl ketone exposure or mechanical wounding. A revised scheme for the uptake of oxygenated VOCs, incorporated into a global chemistry-transport model, predicts appreciable regional changes in annual dry deposition fluxes.

Large quantities of non methane volatile organic compounds (NMVOC) enter the atmosphere via biogenic, pyrogenic and anthropogenic sources. The annual production of NMVOC (~ 1200-1350 TgC/a) likely exceeds that of methane and CO (~500 TgC/a each) *(1, 2)*. Together these gases fuel tropospheric chemistry. Oxidation of NMVOC leads to the formation of aerosols *(3-5)* and modulates the oxidation capacity of the atmosphere *(6)* creating important climate feedbacks *(7)*. One large uncertainty in constraining budgets of NMVOC is the amount of deposition to vegetation, which acts as a major source and sink for organic trace gases on a global scale. This has consequences for constraining secondary species produced in the gas phase, which will either oxidize to

CO and CO_2, condense onto or form organic aerosol (OA) and be rained out, or directly deposit to the surface via dry and wet deposition. Two recent bottom-up assessments of the tropospheric organic aerosol budget *(1, 3)*, based on different assumptions for wet and dry deposition of organic vapors resulted in different predictions of global production rates for secondary organic aerosol (SOA).

Dry deposition schemes parameterize the deposition flux according to

$$F = v_d \cdot C, \qquad \text{(eq.1)}$$

where F represents the deposition flux, C the ambient concentration and v_d the deposition velocity. Deposition velocities are usually treated in analogy to Ohm's Law, where v_d can be expressed as three resistances in series:

$$v_d = \frac{1}{R_a + R_b + R_c}, \qquad \text{(eq.2)}$$

R_a represents the aerodynamic resistance above the surface and has the same value for all constituents. The term R_b is the quasi-laminar resistance to transport through the thin layer of air in contact with surface elements and varies with the diffusivity of a substance. Standard micrometeorological methods and modeling approaches are available to calculate R_a and R_b *(8)*. R_c represents the resistance to uptake by surface elements and has been extensively parameterized for ozone (O_3) and SO_2 *(9)*. Because O_3 immediately decomposes inside plants by reduction, a relative measure of reactivity (f_0 = 0 - 1) accounts for its loss *(9)*. Stomatal resistance (R_s) primarily controls the deposition of highly reactive compounds *(10)*. Due to the lack of observational constraints accounting for the uptake of organic gases occurs in analogy to O_3 and SO_2, solely based on their physio-chemical properties (solubility and reactivity) in the mesophyll. As a consequence all models treat NMVOCs as non-reactive or only slightly reactive species (i.e. f_0=0-0.1) leading to large estimates of R_c *(10)*.

In this report we combine field observations with laboratory experiments and transport modeling to investigate the influence of vegetation on the deposition of oxygenated VOCs (oVOCs). oVOCs represent the most abundant class of organic carbon and profoundly affect the chemical composition in the Earth's oxidizing atmosphere. In six field experiments across a range of ecosystems (Fig. S1), oVOCs deposited at high rates. The sum of methyl vinyl ketone (MVK) and methacrolein

(MAC), which account for about 80% of the carbon in the initial stage of isoprene oxidation, exhibit the fastest deposition rates. R_c for deciduous ecosystems is much smaller than predicted and falls along a trend that would be expected for O_3 (f_0=1) (Fig. 1). This suggests that oVOCs, like O_3, are immediately lost once they enter a leaf through stomata. Tropical ecosystems exhibit the fastest deposition rates (R_c's are 2.6-3.5 times smaller than predicted) and the observed deposition velocities for MVK+MAC are as large as for O_3 (up to 2.4 cm/s). We measured similarly high deposition fluxes for other oVOCs, including acetaldehyde, MVK+MAC, hydroxyacetone, glycolaldehyde, C5-carbonyls, and nopinone (Fig. 2). All oVOCs deposited on the vegetation except acetaldehyde, which exhibited net emissions during a hot period at the beginning of the study because it is also produced by vegetation *(11)*. Due to the bidirectional exchange of acetaldehyde v_d should be regarded as a net deposition velocity. All oVOCs investigated here form during the photochemical oxidation of isoprene and certain monoterpenes. The vertical profiles suggest that deposition mainly occurs via uptake by vegetation elements, with the upper 70% of the canopy (Fig. 2) accounting for more than ~97% of the total deposition flux for all measured oVOCs. After correction for different molecular diffusivities in air, the corresponding R_c's of oVOCs (except acetaldehyde) fall within 25% of O_3. Due to the bi-directional exchange, R_c for acetaldehyde is 60 % higher than O_3 (Fig.2) . Large deposition fluxes imply that the internal concentration (C_i) of these oVOCs is small compared to the ambient concentration (C_a).

To investigate mechanisms that can potentially influence the uptake of oVOCs in particular MVK and MAC we performed a series of leaf cuvette experiments with *Populus trichocarpa x deltoides*. We observed a linear flux-concentration relationship between the uptake (i.e. flux) of oVOCs by a leaf as a function of oVOC concentration (Fig. S3, S5), which is indicative of enzymatic reactions metabolizing oVOCs. The compensation point (C_p) of a compound, defined as the concentration where the net uptake is zero, typically followed an exponential increase with leaf temperature (Fig. S6). When oVOCs form or decompose inside a leaf, the C_p is typically greater than zero, resulting in emission below and uptake above the C_p. The mesophyll resistance (R_m) expressed as a deposition velocity ($v_m = 1/R_m$) was highest between 15 ºC and 20 ºC, dropping significantly above a narrow temperature range between 25 ºC and 28 ºC (Fig.

S6). The light response curves of v_m exhibited a functional form similar to electron transport.

Plants possess the ability to detoxify through various mechanisms [i.e. via oxidative stress or conversion by the aldehyde dehydrogenase (ALDH) family]. As an example, ALDHs are a protein superfamily of NAD(P+)-dependent enzymes known to oxidize a wide range of carbonyls. ALDH enzymes play an important role in the detoxification of aldehydes by oxidizing these to their corresponding carboxylic acids *(12)*. Stress induced upregulation of these and potentially other (e.g. various peroxidase) enzymes could help reduce concentrations of aldehydes and other oVOCs that would otherwise build up to toxic levels.

Based on exposure experiments with *P. trichocarpa x deltoides*, we suggest that chemical and mechanical stress impact uptake rates of acetaldehyde and MVK (Fig. 3). For both plants, v_m for acetaldehyde dropped during fumigation with MVK, but changed little for MVK. The corresponding C_p for acetaldehyde increased during the fumigation period, suggesting increased internal production occurring as a response to oxidative / metabolic stress. During MVK fumigation conversion rates of aldehydes may have also decreased by enzyme saturation or depletion of reactive oxygen species (ROS), which would explain the relatively small change of v_m for MVK during fumigation as opposed to a large increase immediately after fumigation. For the MVK experiment the post-exposure v_m drastically increased for acetaldehyde (~2 fold) and MVK (~20 fold) suggesting short-term upregulation of metabolic activity in response to MVK exposure during the previous days; however v_m decreased after one day in both cases. Because v_m for MVK increased direct or indirect enzymatic reactions rather than purely non-enzymatic reactions (e.g. Michael addition) likely regulated the metabolic consumption. MVK fumigation also resulted in physiological changes. After a certain exposure period, stomatal conductance (G_s) and photosynthesis dropped by 30-50% and 20-50% respectively each day. G_s and photosynthesis however recovered every morning. This corroborates the finding that MVK actively goes through stomata inducing a biological response in the mesophyll.

We did not observe any physiological changes (G_s and photosynthesis) for plant B during the course of the O_3 fumigation experiment. V_m for MVK increased by ~70%

immediately after we exposed plant B to O_3 and gradually increased by another ~25% during the course of the fumigation where it remained after we turned the O_3 supply off (Fig. 3). We observed similar behavior for acetaldehyde. For both compounds v_m remained high for 2 days after stopping the fumigation. A set of experiments inducing mechanical wounding resulted in increased uptake of MVK, qualitatively similar to the chemical exposure experiments. The uptake of acetaldehyde decreased and occurred in parallel with an increasing Cp. This is consistent with the idea that mechanical wounding increases the internal production of acetaldehyde *(11)*. Upon recovery the uptake rates (v_m) for acetaldehyde increased subsequently and at times exceeded the pre-wounding values.

The increase of v_m for acetaldehyde and MVK after (plant A and B) and during fumigation (plant B) imply that these plants responded to acute chemical exposure by upregulating the activity of processes responsible for detoxification. Quantitative polymerase chain reaction (qPCR) identified changes in several characteristic genes indicative of enhanced metabolic activity as a response to chemical and mechanical stress (Table S3). All chemical treatments (MVK, O_3) showed elevated gene expression patterns related to ROS (superoxide dismutase, ascorbate peroxidase). Mechanical wounding and chemical exposure experiments (MVK and O_3) resulted in upregulation of aldehyde oxidase (AAO2) and aldehyde dehydrogenase (ALDH2). We observed elevated levels of p450 cytochrome, typically associated with the oxidation of organic substances, for all chemical treatments along with increases in WRKY transcription factors, encoding proteins involved in plant responses to biotic and abiotic stresses. These changes in gene expression patterns support the gas exchange measurements showing that plants can adjust their metabolism (i.e. v_m) and increase oVOC decomposition as a response to environmental factors.

The presented laboratory and field observations show that oVOCs can be efficiently metabolized by plants through constitutive and induced detoxification mechanisms. Because the general route of atmospheric photo-oxidation of NMVOCs goes through the formation of carbonyls and hydroxycarbonyls these findings have consequences for understanding the atmospheric evolution of these oVOCs. To place these findings on a broader scale we modified the dry deposition scheme for oVOCs in a

comprehensive global chemistry and transport model *(13, 14)*. Fast metabolic conversion of oVOCs was incorporated according to our field observations by setting f_0 to one *(9)*. The total dry deposition flux of organics on a carbon basis increases (by up to 110 %) relative to previous estimates (Fig. 4). Large changes especially occur in tropical regions such as the Amazon, where the annual dry deposition flux increases between 65-85%. Globally, dry deposition of organics increases by about 36%. More importantly, deposition fluxes are substantially altered due to increases (50-100%) in dry deposition of relatively insoluble species [e.g. carbonyls with Henry's Law Constant (HLC) < 50 M/atm] leading to decreases (up to 30%) in wet deposition of certain soluble species [e.g. peroxides with HLCs >300 M/atm (Fig. S8)]. Higher dry deposition of relatively insoluble species also leads to a decrease in dry deposition of certain peroxides due to lower atmospheric concentrations in the gasphase. Modeled oVOC concentrations in the surface layer change substantially (e.g. 30-60%). These results have consequences for capturing the dynamic behavior and repartitioning between NMVOC oxidation products and SOA *(5,14, 15)*. The modifications change OH radical concentrations by up to 15% above the land surface layer (Fig. S11). Tropospheric O_3 concentrations are slightly reduced (e.g. by 1-3%) in the Northern Hemisphere and enhanced in the tropical land regions (e.g. by 0.5-1.5%) (Fig. S10).

Dry deposition of organic trace gases addresses a poorly quantified process in the atmosphere *(3, 10)*. We estimate a lower and upper bound for the annual deposition flux of gas phase oVOCs between 37-56% relative to the annual NMVOC emission flux on a carbon basis (Table S4). It is conceivable that oVOC deposition fluxes to vegetation could increase as a consequence of acute or chronic exposure to high O_3 concentrations in polluted regions *(16)*.

Figures and Figure captions:

Figure 1: Canopy resistance (R_C) for MVK+MAC plotted versus leaf area index (LAI) for six field sites. Black solid line represents dry deposition, where the reactivity factor f_o was set to 1 (maximum deposition). The dotted line shows R_C with a dry deposition that would be conventionally used ($f_0 = 0$). LAI data are plotted as mean +/- SD (n=10); the SD for R_C was calculated as the sum of systematic and random errors associated with turbulent flux measurements (*14*) and the errors associated with instrument precision for wind measurements using a sonic anemometer.

Figure 2: Canopy integrated deposition velocity for ozone (O_3), C_5 carbonyls (C_4CHO), nopinone, glycolaldehyde (GLY), hydroxyacetone (HYAC), MVK+MAC and acetaldehyde (CH_3CHO) as function of normalized canopy height (z/h), where a z/h of one represents the top of the canopy (A). Panel B depicts the leaf area index (LAI) per layer.

Figure 3: Mesophyllic deposition velocity ($v_m = 1/R_m$) for acetaldehyde and MVK; v_m is plotted as a function of cumulative MVK (A) and O_3 (B) uptake. Pre-fumigation levels of v_m (open circles) are inserted at the beginning; post fumigation levels of v_m (open diamonds) are inserted at the end. 95% confidence intervals (n=6 (O_3 fumigation); n=7 (MVK fumigation)) are shown as vertical bars for pre and post fumigation experiments; the dotted lines represent the 95% confidence interval during the fumigation experiment obtained from a polynomial regression (2^{nd} order) depicted by the solid lines.

Figure 4: Relative change of the total annual dry deposition flux of oVOC based on a modified dry deposition scheme in which oVOC are assumed to be rapidly metabolized within the leaf.

References and Notes:

(1) A.H. Goldstein and I. Galbally, Environmental Science & Technology **41**, 1515 (2007).

(2) A. Guenther et al., Atmos. Chem. Phys. **6**, 3181 (2006).

(3) M. Hallquist et al., Atmos. Chem. Phys. **9**, 5155 (2009).

(4) R. Atkinson, and J. Arey, Chemical Reviews **103**, 4605 (2003).

(5) F. Paulot et al., Science **325**, 730 (2009).

(6) J. Lelieveld et al., Nature **452**, 737 (2008).

(7) W.J. Collins et al., Climatic Change **52**, 453 (2004)

(8) C.A. Paulson et al., J. Appl. Meteor. **9**, 857 (1970).

(9) M.L. Wesely, Atmos. Environ. **23**, 1293 (1989).

(10) L. Zhang et al., Atmospheric Environment **36**, 537 (2002).

(11) R. Fall, Chemical Reviews **103,** 4941 (2003).

(12) H.H. Kirch et al., Trends in Plant Science **9**, 371 (2004).

(13) L. K. Emmons et al., Geosci. Model Dev. **3**, 43 (2010).

(14) Materials and methods are available on *Science* online

(15) J.L. Jimenez et al., Science **326**, 1525 (2010)

(16) K. L. Denman et al., in S. Solomon et al., IPCC 4th Assessment Report (Cambridge Univ. Press, Cambridge, 2007), chap. 7.

(17) The National Center for Atmospheric Research is operated by the University Corporation for Atmospheric Research under sponsorship from the National Science Foundation.

SOM Text
Figs. S1 to S16
Tables S1 to S4
References S1 to S59

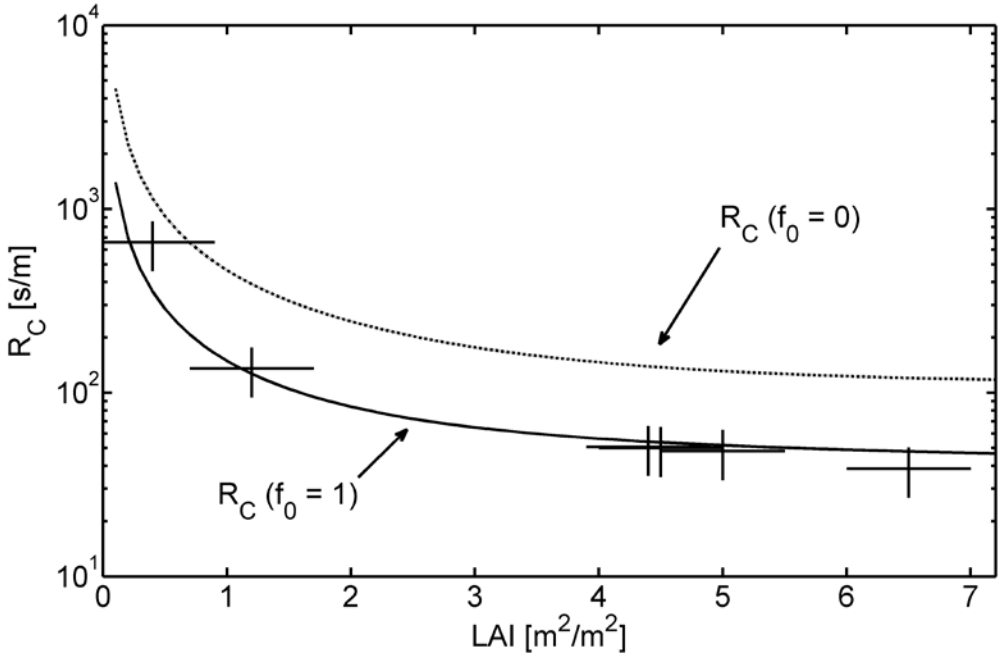

Figure 1

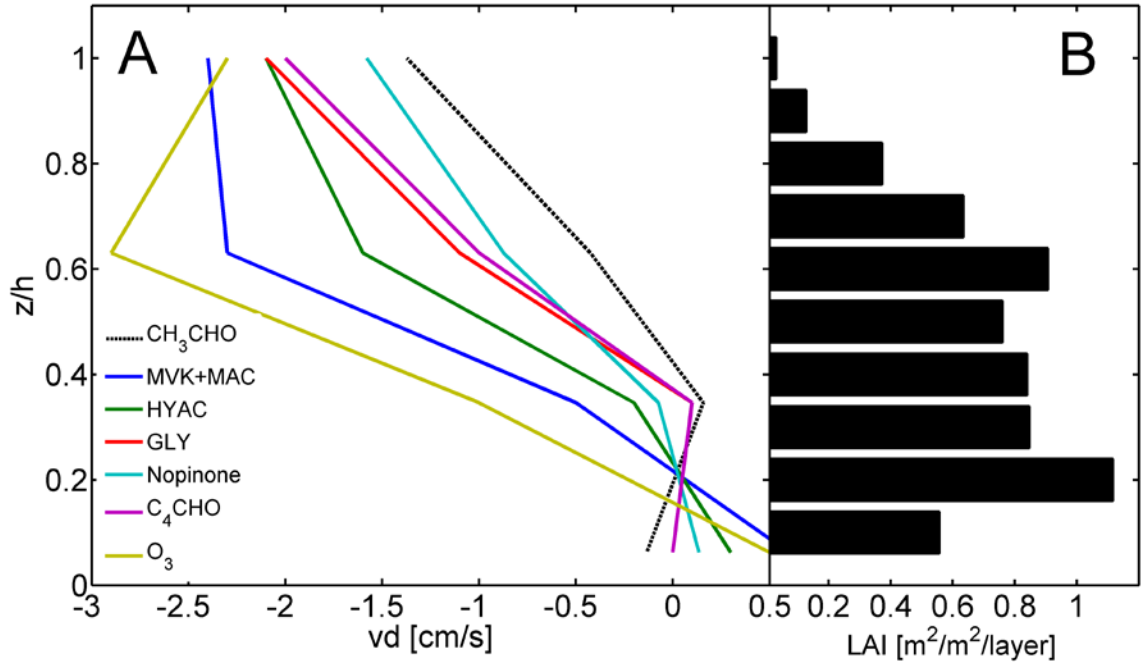

Figure 2

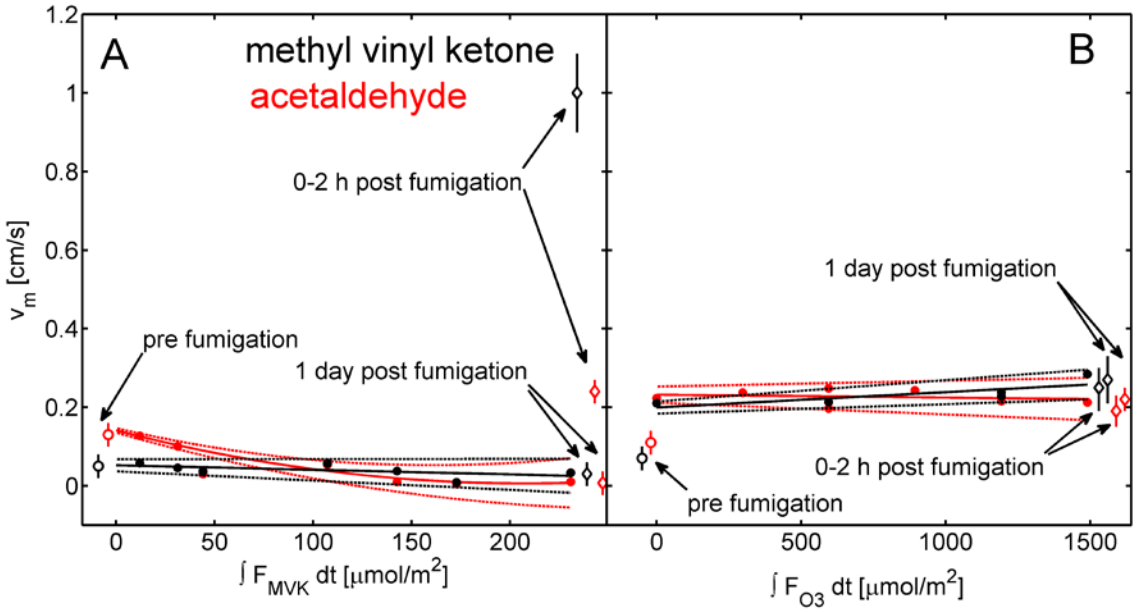

Figure 3

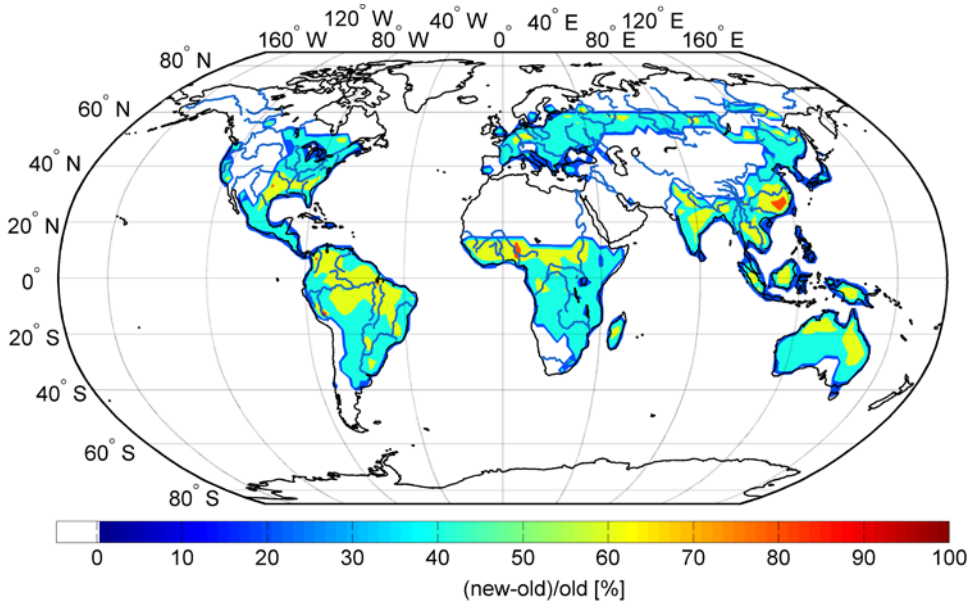

Figure 4

Supporting Online Material

Efficient atmospheric cleansing of oxidized organic trace gases by vegetation

T. Karl[1], P. Harley[1], L. Emmons[1], B. Thornton[2], A. Guenther[1], C. Basu[2], A. Turnipseed[1] and K. Jardine[3]

[1] National Center for Atmospheric Research, Boulder, CO, USA.

[2] School of Biological Sciences, University of Northern Colorado

Greeley, CO, USA

[3] Biosphere 2, University of Arizona, Tucson, AZ, USA.

This file includes:

SOM Text
Figs. S1 to S11
Tables S1 to S4
References S1 to S53

1. Field sites

Six different field experiments were conducted between 2003 and 2009 at sites representing a wide range of ecosystems (Figure S1, Table S1).

Table S1: Field Sites

Field Study	***Year***	***Season***	***Ecosystem***
CELTIC (a)	2003	Dry Season	Tropical rainforest
CELTIC (b)	2003	Summer	Mixed temperate forest
TROFFEE	2004	Dry Season	Tropical rain forest
UMBS 2005	2005	Summer	Temperate deciduous forest
AMAZE	2008	Wet Season	Tropical rain forest
CREATIVE	2009	Summer	Semiarid shrubland

The first campaign (CELTIC 2003a) of the Chemical Emission, Loss, Transformation and Interaction within Canopies (CELTIC) field experiment took place at the La Selva Biological Station (10.43º N, 83.93º W), which is situated in the lowland tropical wet forests of the canton Sarapiqui, province of Heredia, Costa Rica (S1). The campaign took place in April during the dry season of 2003. The second campaign (CELTIC 2003b) was conducted at the Duke Forest C-H2O, an experimental loblolly pine (Pinus taeda) plantation with sweetgum (Liquidambar styraciflua) understory in

North Carolina (35.98º N, 79.09º W). The site is the location of the Duke University FACE (Free Air CO2 Enrichment) Study. More specific details can be found in Katul et al. (1999) (S2).The study took place in July 2003.

The tropical forest and fire emissions experiment (TROFFEE 2004) (S3) was conducted on an instrumented flux tower (2.61º S, 60.21º W) situated 60 km NNW of Manaus in Central Amazonia during the dry season in September 2004. The vegetation cover consists of primary tropical rainforest.

The fourth campaign (UMBS 2005) was conducted at the PROPHET Tower (at the University of Michigan Biological Station (UMBS)) (45.5º N, 84.7º W) (S4). The site is situated in the transition zone between the mixed hardwood and boreal forests. Bigtooth aspen (Populus grandidentata) and red oak (Quercus rubra) dominate within the footprint of the tower. Measurements were conducted in August 2005.

The Amazonian Aerosol Characterization Experiment (AMAZE 2008) (S5) took place during the wet season in February 2008. The site (2.59º S, 60.21º W) is located in the Reserva Biologica do Cuieiras and managed by the Instituto Nacional de Pesquisas da Amazonia (INPA) and the Large-Scale Biosphere-Atmosphere Experiment in Amazonia (LBA). The vegetation cover consists of primary tropical rainforest.

The sixth campaign (CREATIVE 2009) was conducted in a creosote (Larrea tridentate) shrubland ecosystem in Southern Arizona (31.91º N, 110.83º W). Measurements were performed during the month of June in 2009.

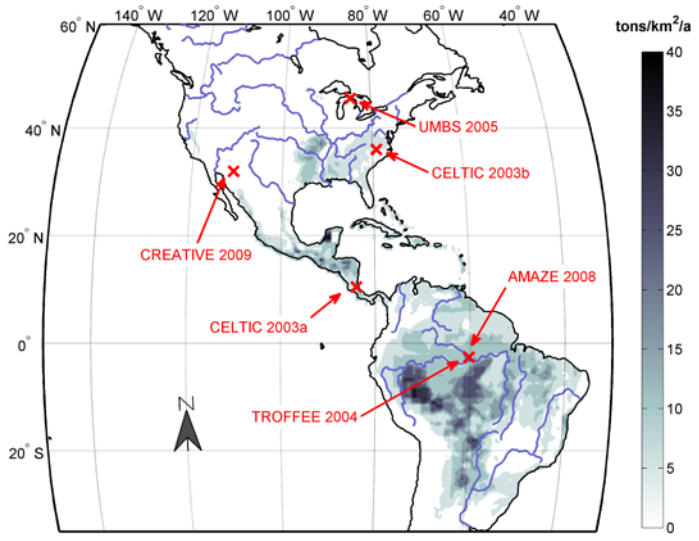

Figure S1 shows the locations for the six field experiments and a map of estimated isoprene emissions.

2. Instrumentation

2.1 PTRMS

A Proton-Transfer-Reaction Mass Spectrometer (Ionicon, Austria) (PTR-MS) was used for eddy covariance and gradient measurements of selected NMVOCs. The

instrument is based on soft chemical ionization using protonated water ions (H_3O^+). It combines the advantage of online analysis while maintaining linearity and low detection limits (S6, S7). A detailed description about operating conditions and instrument validation was previously documented (S8). In this work the instrument was typically operated between 2 and 2.5 mbar drift pressure and 540-600 V drift voltage and calibrated using two multicomponent ppmv NMVOC standards: NMVOC standard 1 contained a mixture of methanol, acetonitrile, acetaldehyde, acetone, isoprene, methyl vinyl ketone, methyl ethyl ketone, benzene, toluene, m,o,p xylenes and camphene; VOC standard 2 contained a mixture of benzene, toluene, m,o,p xylenes + ethylbenzene, chlorobenzene, trimethylbenzenes, dichlorobenzenes and trichlorobenzenes. The instrument sequentially sampled through six independent ¼" inch Teflon (PFA) sampling lines mounted at 2, 10.9, 16.7, 23.9, 30.3, and 39.8 m on a 40 m tall tower. A valve switching system changed sampling lines every 5 minutes and cycled through the entire gradient over a 30 minute period. Gradients were calculated from the 5 minute averages. High flow rates through the sampling lines resulted in delay times of less than 8-12 seconds, measured by spiking a NMVOC pulse at each sampling inlet. Isoprene and the sum of MVK and MAC were measured at ion channels m/z69 and m/z71 respectively. Hydroxyacetone was monitored on ion channel m/z75. The detection limits for isoprene, MVK+MAC and hydroxyacetone for a 5 s integration time were 10, 5 and 5 pptv respectively. These particular sensitivities corresponded to proton-transfer reaction rate constants of 2×10^{-9} , 3×10^{-9} and 3.5×10^{-9} cm^3/s respectively. The sum of acetic acid and glycolaldehyde was observed on m/z 61. Nopinone, an oxidation product of beta-pinene, was measured on m/z 139 (S9, S10) and the sum of methyl-furan and C_5 carbonyls were observed on m/z 83. No calibration standards were available for the latter five compound classes, but the relative instrument fragmentation patterns were verified using pure vapor injection based on liquid standards (SigmaUltra, Sigma Aldrich, Milwaukee, WI). Proton-transfer-reactions typically occur at the collisional limit; without specific calibration standards the concentrations can be calculated within 40% accuracy. By defining a deposition velocity (flux divided by the concentration) the uncertainty of calibration factors cancels out assuming instrument linearity and we exploit this fact for the analysis in this paper.

2.2 GC-MS and GC-FID

Air samples were collected on solid absorbent cartridges that were stored at approximately 0 ºC until analysis at NCAR Boulder laboratory, except during transit to the laboratory, when they were at ambient temperature for approximately 1 day. The analytical technique for four campaigns (CELTIC 2003a, CELTIC 2003b, TROFEE 2004, UMBS 2005) consisted of collection on carbotrap and tenax cartridges, thermal desorption using an NCAR-made system, and analysis on an gas chromatograph with mass spectrometric detection (GC-MS) described in detail by Greenberg et al., (1994) (S11). The GC-MS system used for AMAZE 2008 was a Hapsite Smart (Inficon, East Syracuse NY, USA) with a 30 m x 0.32 mm ID 1 mm film DB-1 column, temperature programmed from 40 to 200 C at 3 C per min. Samples from CREOSOTE 2009 were collected on carbograph 5TD and Tenax GR cartridges, thermally desorbed using a Unity/Ultra II (MARKES, Llantrisant, UK), passed through a a 30m DB5 column in an

Agilent 7890A series Gas Chromatograph temperature programmed with an initial hold of 1 min at 35 oC and subsequent temperature rampings of 6 °C/min to 80 °C, 3 °C/min to 155 °C, 10 °C/min to 190 °C, 25 °C/min to 260 °C with a final hold of 5.2 min., and analyzed with an 5975C series Gas Chromatograph/electron impact ionization mass spectrometer with a triple-axis detector and a Flame Ionizaton Detector. VOC were quantified with respect to NIST traceable standards as described by Greenberg et al. (1994) (S11).

2.3 Ozone and leaf area index

During AMAZE, Ozone (O_3) concentrations were measured via the 6-level sampling manifold. Ozone was measured by UV absorbance (2B Technologies, Model 205) every 10 s and then averaged over the entire 5 minute sampling time on each level, excluding only the first 15 seconds to insure adequate flushing of the connecting gas lines. The ozone analyzer was compared with laboratory instruments both prior to and following the experiment and found to agree with ±5% with a detection limit of 2 ppbv. It was zeroed periodically by placing an ozone scrubber on the 1.5 m inlet.

The leaf area index was measured indirectly using the LAI2000 (LI-COR, Lincoln, Nebraska).

2.4 Environmental chamber

Leaf enclosure measurements were conducted inside a controlled environment plant growth chamber (Conviron, Model BDW40, Winnipeg, CA). Air temperature was held constant at 25^{o}C, and plants experienced a 12 hr photoperiod, with photosynthetic photon flux density at experimental leaf height maintained at 380 μmol m^{-2} s^{-1} between 0700 and 1800 hrs, when measurements were conducted. All lines were equilibrated at the same temperature inside the growth chamber. Sampling lines exiting the chamber to oVOC sampling systems were kept at 50ºC.

2.5 Gas exchange measurements

2.5.1 Ecoyphysiological measurements CO_2, H_2O

Measurements of net photosynthesis, stomatal conductance and oxygenated volatile organic compounds (oVOC) exchange were measured using a dynamic flow-through gas exchange system constructed inside the plant growth cabinet. Single leaves were inserted into each of two home-made, temperature-controlled, fan-stirred glass enclosures (volume=550 cm^3), and a controlled flow (Mass Flow Controllers, Model UFC-8100; Unit Instruments, Yorba Linda, CA) of zero air supplemented with pure CO_2 to a final concentration of approx. 420 ppm was passed through each chamber. Absolute humidity of air entering the chambers was varied by mixing dry and humidified zero air, and measured using a temperature and relative humidity probe (Model CS215, Campbell Scientific, Logan, UT). CO_2 concentration of air entering the chambers was measured with an infrared gas analyzer (Model LI-820, Li-Cor, Lincoln, NE), and the change in both CO_2 and water vapor concentrations across the chambers was measured using a

second infrared gas analyzer (LI-6262, Li-Cor) in differential mode. Photosynthetic photon flux density incident on each leaf was measured using a quantum sensor (Model SQ-110, Apogee Instruments, Logan, UT) and leaf temperatures using thermocouples (Type T) appressed to the abaxial side of the leaf. Knowing the flow rate of air through each chamber, the change in CO_2 and H_2O concentrations across the chamber and the amount of leaf area enclosed, rates of net photosynthesis, evapotranspiration and stomatal conductance were calculated using the equations of von Caemmerer and Farquhar (1981) (S12).

2.5.2 oVOC exchange measurements

A ppm level gas standard containing a mixture of different oVOCs was dynamically diluted to concentrations between 0.5 and 50 ppbv. The mixture was added to the air flow entering the two leaf cuvettes. An automatic valve switching system allowed to sample the concentration at the in- and outlet of each cuvette. The dilution was automatically adjusted every 5 minutes in 6 steps, so that a compensation point curve could be obtained every 30 minutes. Figure S5 shows a typical example for a leaf temperature at 15ºC. For fumigation experiments an ozone generator was placed in line with the airflow going to a leaf cuvette. The oVOC mixture was added downstream of the ozone generator. Alternatively MVK was added to the ingoing flow. The resulting concentrations at the leaf cuvette inlets during fumigation experiments were 120-180 ppbv and 170-220 ppbv for ozone and MVK respectively.

We performed background tests by introducing oVOC mixtures through the system without plant samples. We did not observe any losses in the cuvette and sampling setup.

2.6 Gene Expression: Methods and Results

2.6.1 Biological material.

Populus trichocarpa x deltoides saplings were maintained at the National Center for Atmospheric Research, Boulder CO. Prior to treatment, and 24 hours after treatment with ozone (O_3), methyl vinyl ketone (MVK) or mechanical wounding, whole, intact leaves were collected, snap frozen in liquid nitrogen and transferred to a -80 ^{0}C freezer until needed for analysis.

2.6.2 RNA isolation and purification.

RNA extraction buffer was prepared using 2% Cetyltrimethylammonium Bromide(CTAB) (w/v), 2 M NaCl, 25 mM ethylenediaminetetraacetic (EDTA); 100 mM Tris-HCl (pH 8.0) and 2% polyvinylpyrrolidone (PPV) (w/v). The solution was autoclaved to sterilize and then stored at room temperature. All mortars, pestles and spatulas were first autoclaved and then treated with RNase Away (Sigma-Aldrich, St. Louis, MO). RNase Away was used to treat all gel boxes, combs, pipetters, gloves and workspace. Only certified nuclease-free, barrier tips, water and microcentrifuge tubes

were used for RNA extraction. Centrifugations were carried out at room temperature in a tabletop microcentrifuge.

Poplar leaves were removed from storage and immediately ground in liquid nitrogen using mortars and pestles and transferred to a 1.5 mL microcentrifuge tube. To the ground leaf material, 1000 µl of CTAB extraction buffer and 25 µl of β-mercaptoethanol were added. The mixture was vortexed for 25 seconds and then incubated in a water bath at 65°C for 5 minutes. To ensure total lysis of cells, and binding of polyphenolics and polysaccharides, the mixture was vortexed briefly every 3 minutes during incubation. To collect plant debris, the tubes were centrifuged for 5 minutes at 14,000 rpm. The supernatant was decanted into a new tube, and to it 600 µl of chloroform:isoamyl (24:1) was added. The tube was capped, hand shaken for 10 seconds to mix, and then centrifuged for 6 minutes at 14,000 rpm to separate the mixture into an aqueous upper phase and an organic lower phase. The upper aqueous phase was carefully pipetted into a new tube and the chloroform:isoamyl separation was repeated. The final aqueous phase was removed to a new tube and a volume of 3/10 the aqueous phase of molecular grade 5 M ammonium acetate plus an equal volume (aqueous plus ammonium acetate) of 100% sterile-filterized isopropyl alcohol was added. RNA was allowed to precipitate overnight at -20 °C. The RNA pellet was washed twice using 70% ethanol and then resuspended in nuclease-free water. Trace DNA was removed with DNaseI (Fermentas, Glen Burnie, MD) according to the manufacturer's instructions, and enzyme activity was deactivated by adding 1 µl EDTA and incubating for 10 minutes at 65°C. RNA was quantified by NanoDrop spectrophotometer.

2.6.3 Reverse Transcription, Primer Design and Quantitative PCR.

First strand cDNA was synthesized using 1 µg total RNA and iScript™ Synthesis Kit (Bio-Rad Laboratories, Hercules, CA, cat. # 170-8891) with a mixture of random hexamer and Oligo dT primers, according to the manufacturer's instructions. Primers for genes known to be involved in the detoxification and repair process from ozone injury were designed from Poplar ESTs, obtained from the National Center for Biotechnology Information (www.ncbi.nlm.nih.gov), using Primer3 software (S13, S14). Primer sets are shown in Table S2. The presence for potential secondary structure formation between primers was analyzed using Beacon Designer Free Edition software (Premier Biosoft, Palo Alto, CA). Target amplicons were evaluated for secondary structures using IDT SciTools mFold software (Integrated DNA Technologies, Coralville, IA). Ubiquitin (UBQ) was chosen to use as a housekeeping gene based on previous analysis by Brunner et al. (2004) (S15) which demonstrated that UBQ expression remains stable and consistent among different Poplar tissue samples.

All reagents were mixed under a sterilized and UV-treated hood, using aerosol barrier tips. A master mix of iQ™ SYBR® Green (Bio-Rad) was made according to the manufacturer's instructions and alloquated in 25 µl volumes with 1 µl of cDNA. Technical replicates were repeated in triplicate, and each set of primers included a technically replicated, no template control. Real-time PCR was performed on an iQ5 real-time PCR detection system (Bio-Rad) using the following parameters: 95°C for 3 min; 50 cycles of 95°C (for 30 s), 60°C (for 30s), 72°C (for 30s). Specificity of the amplifications was verified by dissociation curve analysis, by temperature ramp.

Quantifying the relative changes in gene expression was performed using the ΔΔCT method (S16).

Table S2: Poplar primers for SYBR® green based quantitative PCR.

ID	Gene Name	Forward	Reverse	Amplicon Length
XM_002322287.1	**MsrA**--Methionine sulfoxide reductase	GACCCAACAATCCCACAAG	CAACACCCCAAAAACAACCA	91
EF405967.1	**SOD**—Cu-Zn Superoxide dismutase	CTCTCAAACTCAACAAACAAACATAC	CCACTCACACCTTCACTGCT	120
XM_002328049.1	**AAO2**—Aldehyde oxidase 2	GAGCAGATAGAAAGAGAAACGAAAA	CAATACAAGCACCACAACCAC	169
EF631997.1	**ALDH2**-Aldehyde dehydrogenase	GACACTGCCAACACCCTTTC	TCCCTTTTCTCTACCATTTCCA	126
E12805.1	**ACS**--aminocylcopropane carbonic acid synthase	CATTAGGGAAAGCAAAGGAGA	TCAAATCCATCCACAAAAACA	122
XM_002313470.1	**APX**--Ascorbate peroxidase	TGAGTGGGGAGAAGGAAGG	TAATCGGCAAAGAAAGCATC	121
AY167040.1	**ACO1**--1-aminocyclopropane-1-carboxylic acid oxidase	CCCCTGTCTCCCTCTCTTTC	CCACTCCTCGCATCCATT	143
XM_002299061.1	**P450**—Cytochrome p450	GCACACCATTTTGACATCTTTC	CAACCAACCGAATCTCTTCC	121
XM_002314438.1	**DHQ**-- dehydroquinate dehydratase/ shikimate dehydrogenase	TCCTTTTCCTCTCTCTCTTTTCTTT	TCCATCTTTTCTTTCTTTCTTTTTG	111
EF051079.1	**WRKY**-- WRKY transcription factor	GCGAGGGTTTGAATGATGAA	CGGCTCTCTCTGTCTCTTCTG	119

2.6.4 Gene Expression Results

Populus trichocarpa x deltoides saplings were fumigated with either O_3, or MVK, or were mechanically wounded, and analysis of differential gene expression was used to survey the expression levels of 10 genes known to be involved in signaling, detoxification or repair from reactive oxygen species (ROS) and reactive electrophile species (RES) (Table S3).

In the poplar trees there was a ~2 fold or greater induction of both ACS and ACO gene transcripts in response to O_3 and MVK treatments or mechanical wounding (Table S3). This data is consistent with microarray analysis of *Arbidopsis thaliana* exposed to MVK, where ACO was induced 2 to 3 fold (S17) and increases in ACS induction in tobacco plants exposed to O_3 (S18). In all chemical treatments, the WRKY transcription factor was upregulated. In a similar fumigation treatment of poplar hybrid clones with O_3, WAK receptor-like protein kinases and WRKY transcription factors were both activated (S19). Two of the major ROS scavenging enzymes were evaluated: superoxide dismutase (SOD) and ascorbate peroxidise (APX). The levels of both SOD and AXP transcripts increased across the chemical treatments, indicating that the steady-state levels of ROS had been disrupted. An increase in ALDH transcriptomes was also seen in the chemical treatments. As previously reported, ALDH activities are considered to be an efficient defense strategy to eliminate toxic aldehydes caused by ROS (S20, S21). The genome of *Populus trichocarpa* contains five methionine sulfoxide reductase A (MsrA) genes. The presence of MsrA is known to play protective roles in the cellular response to

oxidative stress and protein repair (S22). Transcript levels of MsrA3 was found to be elevated across all treatments.

Table S3: Gene expression patterns for three different treatments (O_3, MVK and mechanical wounding (m.w.)). Upregulated genes are listed, where the twofold ratios are defined as $2^{(-\Delta\Delta Ct)}$. Ratios above 2.0 (99.9% confidence) are highlighted in red, and ratios between 1.5 (99.0% confidence) and 2.0 are highlighted in green. The mean is calculated from three individually fumigated leaves on three trees (n=4), where the standard deviation (SD) is defined as $SD_{foldchange} = (\ln 2)(stdev_{\Delta\Delta Ct})(2^{(-\Delta\Delta Ct)})$.

	MsrA	***AAO2***	***ALDH2***	***SOD***	***APX***	***ACS***	***ACO2***	***P450***	***DHQ***	***WRKY***
O_3	3.4±0.6	9.2±3.7	20.0±9.2	1.8±0.3	4.4±0.8	2.4±0.1	10.9±1.4	3.4±0.5	3.6±2.0	**4.9±0.8**
MVK	7.6±4.2	1.7±0.5	8.5±3.0	2.4±0.8	4.4±1.4	1.2±0.2	5.4±3.0	26.7±11.4	2.0±0.7	**6.9±2.5**
m. w.	**1.5±0.2**	**2.1±0.6**	**2.0±0.3**			**2.4±0.8**	**5.1±2.6**			

2.7 Statistics used for error analysis

The standard deviation (SD) for LAI measurements was based on five repetitions performed at two field sites; these 10 independent samples are used to infer an instrument specific random error (SD) shown in Figure 1. SD for ecosystem scale flux measurements was calculated as the sum of systematic and random errors associated with turbulent flux measurements and errors associated with instrument precision for wind measurements using a sonic anemometer (5%). The error for flux measurements due to geophysical variability was calculated according to Wesely and Hart (1985) (S23):

$$\frac{\partial F}{F} = \sqrt{\frac{12 \cdot z}{T \cdot u}} \text{ (unstable conditions),} \qquad \text{(eq. S1)}$$

and,

$$\frac{\partial F}{F} = \sqrt{\frac{20 \cdot z}{T \cdot u}} \text{ (neutral conditions),} \qquad \text{(eq. S2)}$$

where T is the averaging period (e.g. 30 minutes), z is the height above ground, and u is the wind speed.

Biological replication:

For enclosure measurements, we generally used three leaves on two plants for both fumigation experiments (e.g. Fig. 3) and mechanical wounding experiments. We define the experimental setup as six independent replicates since fumigations were performed individually on each leaf (n=6). The MVK fumigation experiment included one additional leaf compared to the ozone treatment. Pre and post fumigation experiments were therefore conducted on six (O_3) and seven (MVK) leaves. During the O_3 fumigation experiment, we excluded one MVK sample due to instrument problems, which results in n=5 for MVK during the O_3 fumigation. For the genetic analysis, we fumigated (or mechanically wounded) four individual trees and collected 1 leaf from each

treated tree (1 leaf was also collected as control prior to each experiment). The genetic analysis was performed by technical replication. In short, RNA was collected independently from each leaf, and cDNA was created separately for use in qPCR analysis. Quantitative, real-time PCR was performed in triplicate on each cDNA sample for each of the 10 genes analyzed.

3. Eddy covariance and ILT flux measurements

Ecosystemscale fluxes of oVOCs were calculated based on eddy covariance measurements (S24) and concentration gradients throughout the canopy by applying an Inverse Lagrangian Transport Model (ILT) (S25, S26, S27). Briefly, eddy covariance, disjunct eddy covariance and virtual disjunct eddy covariance methods (S28, S29, S30) extensively used to measure VOC fluxes using PTRMS. All approaches are mathematically based on the covariance between vertical wind velocity and concentration fluctuation according to:

$$F = \overline{c' \cdot w'} \qquad \text{(eq. S3)}$$

where F is the VOC flux, c' is the instantaneous concentration and w' is the instantaneous windspeed. Above forests the covariance is typically calculated for 30 minute periods. Eddy covariance is widely used in micrometerological applications and we refer to the specialized literature (S24).

VOC fluxes based on the ILT model were computed according to,

$$\vec{C} - C_{ref} = \vec{D} \cdot \vec{S} \qquad \text{(eq. S4)}$$

where C is the VOC concentration ($\mu g/m^3$) vector for each level, C_{ref} is the VOC concentration ($\mu g/m^3$) at reference height (e.g. 14 m), D (m) represents a dispersion matrix and S ($mg/m^2/h/m$) the resulting VOC source/sink vector. D can be expressed as a function of Lagrangian timescale (Tl) and profiles of the standard deviation of the vertical wind speed (σ_w) divided by the friction velocity (u*). The calculation was performed using a 10 x 4 dispersion matrix. Integration over all source and sink terms (S) yielded the canopy scale VOC flux ($mg/m^2/h$). Fluxes were calculated for 30 minute intervals. The parameterization of D was based on turbulence measurements inside and above the canopy (σ_w/u^*, where σ_w is the standard deviation of vertical wind speed and u* is the friction velocity) and calculated using the far- and near-field approach described by Raupach (1989) (S25). The Lagrangian timescale Tl (s) was parameterized according to Raupach (1989) (S25). Figure S2 shows a typical example for conditions in the Amazon during the 2008 wet season.

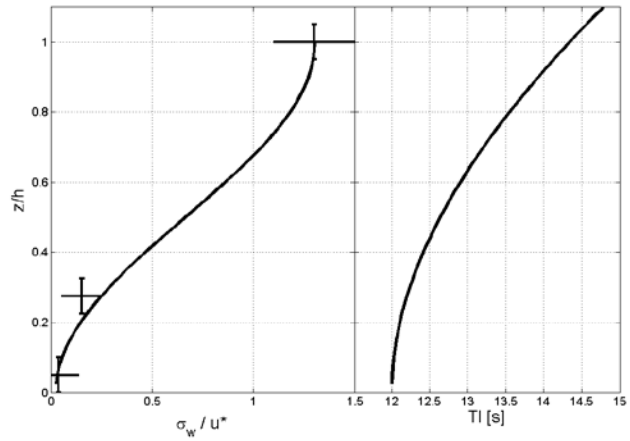

Figure S2: Measured turbulence profile (σ_w/u*) and fitted parameterization according to Raupach (1989) (S25) as a function of normalized canopy height (z/h) during the AMAZE study, 2008 (left panel). Lagrangian timescale (Tl) as a function of z/h (right panel). X-errorbars represent 1 SD according to eq. S1 (unstable conditions) or S2 (stable conditions). Y-errobars represent 1 SD (n=3).

Reaction rates of oVOCs with respect to OH (the main oxidant; reaction with ozone or NO_3 are considered negligible for oVOCs) investigated here are a factor of 3 to 10 lower than for example for isoprene. This leads to a chemical lifetime of 1.6 – 6 hours for an OH density of 5 x 10^6 molecules/cm^3 (upper limit: e.g. in tropical PBL S31). The turnover time in canopies investigated here (e.g. based on typical ramp structures) is on the order of 1-5 minutes. Taking an upper limit of an incanopy OH concentration of 2 x 10^6 molecules/cm^3 (e.g. 50% of PBL concentration; S32), the chemical loss inside the canopy for the most reactive oVOC investigated here (MAC) is less than 2%.

Figure S3 shows a typical example obtained from eddy covariance fluxes in the Amazon during the 2004 dry season. MVK+MAC deposition fluxes are plotted as a function of ambient mixing ratios. The slope is associated with a deposition velocity.

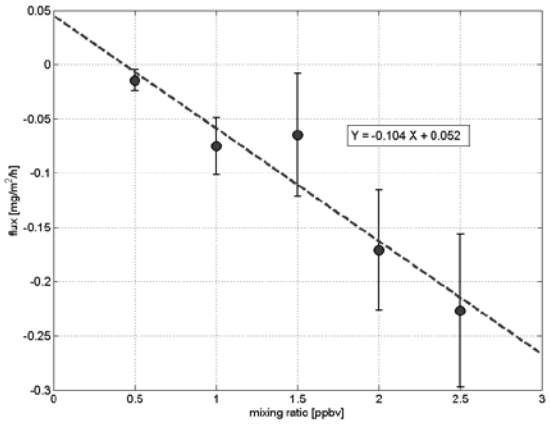

Figure S3: Study average deposition flux of methacrolein and methyl vinyl ketone by eddy covariance in the Amazon between 10 and 14 local time (LT) during the 2004 dry

season. Errorbars represent 1 SD according to eq. S1 (unstable conditions) or S2 (stable conditions).

4. R_a, R_b and R_c calculations

The aerodynamic resistance R_a is obtained from turbulent measurements according to:

$$R_a(z-d) = \frac{1}{\kappa u_*}\left(\ln\left(\frac{z-d}{z_0}\right) - \psi_H(\zeta)\right) = \frac{u(z-d)}{u_*^2} - \frac{\psi_H(\zeta) - \psi_M(\zeta)}{\kappa u_*} \quad \text{(eq. S5)}$$

where k is the von Kármán constant (0.4), u* is the friction velocity, z is the height above ground, d is the displacement height, ζ is z/L with L the Monin-Obukhov length, z_0 is the roughness height, and Ψ_H and Ψ_M are stability functions (S33).
The boundary layer resistance R_b is calculated according to:

$$R_b = \frac{2}{k \cdot u*}\left(\frac{Sc}{\Pr}\right)^{2/3} \quad \text{(eq. S6)}$$

where Sc is the Schmidt number and Pr the Prandtl number. R_c can then be obtained experimentally from:

$$R_c = \frac{1}{V_d} - \left[R_a(z-d) + R_b\right] \quad \text{(eq.S7)}$$

where v_d is the deposition velocity (= $-F_c/C$). We can also calculate a value of R_c by adopting a 5 layer energy balance model according to the MEGAN framework (S34, S35) similar to Baldocchi et al. (1987) (S36). Stomatal resistances (R_s) are calculated according to the energy balance for shade and sun leaves in each layer. The canopy light environment model is based on Spitters et al. (1986) (S37), Goudriaan and van Laar (1994) (S38) and Leuning (1995) (S39). Mesophyllic and cuticular resistances are adopted according to recommendations by Wesely (1989) (S40) and Zhang et al. (2002) (S41). Assuming that the measured R_c for water vapor is predominantly controlled by stomatal resistance, Figure S4 shows a comparison between average noon time measured and modeled stomatal resistance R_s.

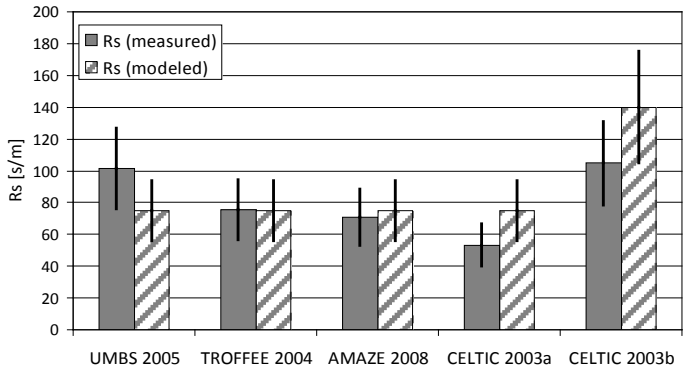

Figure S4: Modeled and measured noon-time R_s for different field experiments. Modeled values are representative for clear skies conditions according to a parameterization recommended by Wesely (1989) (S40). Errorbars represent 1 SD according to eq. S1 (unstable conditions) or S2 (stable conditions).

5. Compensation point measurements in the laboratory

According to Fick's law the flux inside a plant across stomata can be approximated as:

$$F = \frac{1}{\frac{1}{D_x \cdot G_s} + R_m} \cdot (C_a - C_i) \qquad \text{(eq. S8)}$$

where F is the measured flux, D_x is the ratio of the diffusivity between a VOC and water (D_x (=D_{h2o}/D_{VOC})), G_s is the stomatal conductance, R_m represents the mesophyll resistance, C_a is the ambient concentration and C_i is the internal concentration. In analogy to CO_2 the mesophyll resistance (R_m) is a measure of both diffusion and biochemistry. Figure S5 shows a typical example for a compensation point (C_p) determination for acetaldehyde and MAC obtained from laboratory experiments with *populus deltoides*. In this case the C_p is close to 0 ppbv for methacrolein and 1 ppbv for acetaldehyde. Similar results were obtained for MVK and were previously reported for MAC and crotonaldehyde (S42)

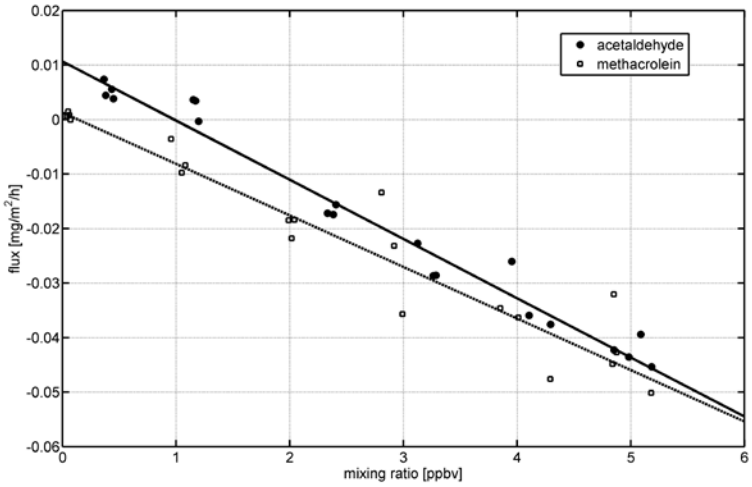

Figure S5: Flux measured as a function of mixing ratio for acetaldehyde (circles, solid line) and methacrolein (squares, dashed line) at 15ºC and 350 μE/m^2/s.

Figure S6 summarizes findings from oVOC exchange measurements for acetaldehyde and methacrolein (3 leaves x 2 plants). Panel A (B) depicts the temperature dependence of the compensation point C_p for acetaldehyde (methacrolein), which follows an exponential increase. No significant variation of C_p as a function of photosynthetically active radiation (PAR) was observed for acetaldehyde and methacrolein (panels C and D

respectively). Panels E and D show the normalized mesophyllic velocity (v_m=1/R_m) expressed as a function of temperature. The mesophyllic velocity v_m was highest at temperatures between 15 ºC and 20 ºC, dropping significantly above a narrow temperature range between 25 ºC and 28 ºC. This behavior is consistent with multiple interacting enzymes, which is for example also used to describe the temperature dependence of a complex sequence of enzyme-mediated reactions leading to carbon assimilation (S43). The mesophyllic velocity (v_m) is plotted as a function of PAR in panels G and H for acetaldehyde and methacrolein respectively. The mesophyllic deposition velocity (v_m) follows a functional form similar to electron transport, with the exception that v_m drops to almost zero at very low light (<150 PAR). A generic equation of the form:

$$v_m = \frac{a \cdot b \cdot PAR}{\sqrt{1 + a^2 \cdot PAR^2}}, \qquad \text{(eq. S9)}$$

was fitted to the measurements. The parameters a and b exhibited values of 1.5e-2 (3.4e-3) and 0.14 cm/s (0.08 cm/s) for acetaldehyde (methacrolein) respectively. The observations suggest that these oVOCs are consumed by enzymatically driven reactions.

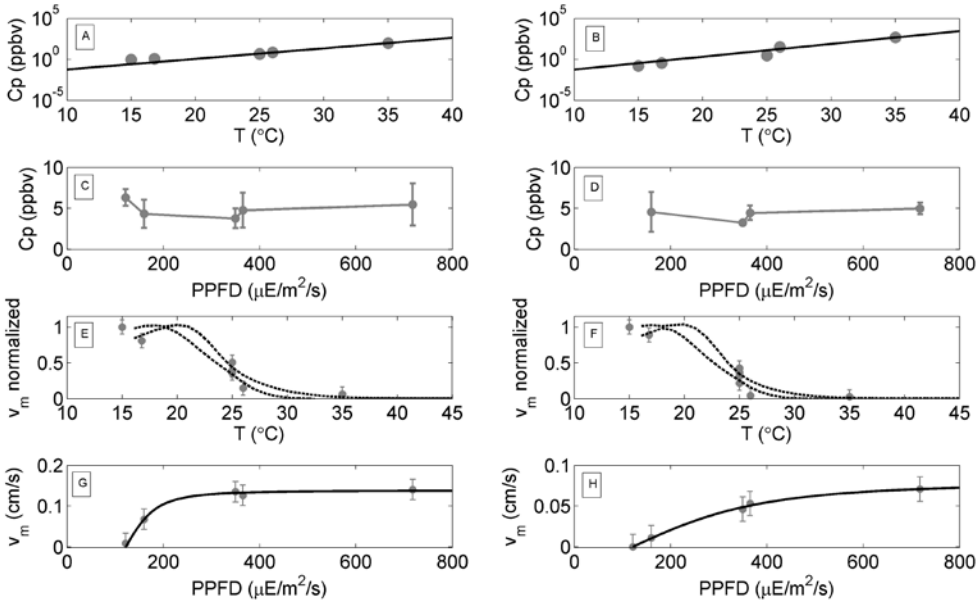

Figure S6: Summary of exchange measurements for acetaldehyde (left) and methacrolein (right). Panels A and B: Cp as a function of temperature; panels C and D: C_p as a function of PAR; panels E and F: v_m as a function of temperature (dashed lines represent 95% confidence interval); panels G and H: v_m as a function of PAR. All errorbars represent 1 SD (n=6).

6. Global Model MOZART-4

The MOZART-4 (Model for Ozone and Related chemical Tracers, version 4) global model has been described in great detail by Emmons et al. (2010) (S44). Here we briefly review the deposition parameterization.

6.1 Dry and wet deposition

Dry deposition velocities are determined online in the model, based on the resistance-based parameterization of Wesely (1989) (S40), Walmsley and Wesely (1996) (S45), Wesely and Hicks (2000) (S46). The calculation of surface resistances uses the vegetation distribution of Bonan et al. (2003) (S47). The deposition velocity calculation has been extended to take into account special cases for CO, H_2 and peroxy-acetyl-nitrate (PAN). Surface uptake of CO and H_2 has been parameterized using the approach of Sanderson et al. (2003) (S48), which defines the deposition velocity by a linear or quadratic function in soil moisture content (or its logarithm), depending on the land cover type. In the case of PAN, new laboratory experiments have indicated a strong uptake of PAN by leaves (S49). Using the results from that study, leaf uptake of PAN is included depending on vegetation type, based on Sparks et al. (2003) (S50). Wet deposition is taken from the formulation of Brasseur et al. (1998) (S51). In the present modeling study the reactivity factor f_0 was set to 1 for the following oxygenated MOZART-v4 species: CH2O, CH3CHO, GLYOXAL, CH3COCHO, GLYALD, HYDRALD, CH3OH, C2H5OH, CH3COCH3, HYAC, CH3OOH, C2H5OOH, C3H7OOH, CH3COOH, CH3COOOH, ROOH, MACROOH, XOOH, ISOPOOH, ALKOOH, MEKOOH, TOLOOH, TERPOOH, MVK, MACR. A number of these species represent products from lumped hydrocarbons (e.g., HYDRALD, ALKOOH). Further information on the MOZART-v4 species and chemistry mechanism can be found in Emmons et al., (2010) (S44).

Based on our field measurements fast metabolic conversion of oVOCs was incorporated by forcing the reactivity factor f_0 to 1, according to Wesely (1989) (S40); in particular this modification was applied to equations 6, 7, 8 and 9 (S40), describing mesophyllic, upper, lower and ground canopy resistances.

6.2 Changes in wet deposition of organics

Figure S7 shows the resulting change in wet deposition fluxes for all organics (calculated on a carbon basis) after incorporating modifications to the dry deposition scheme.

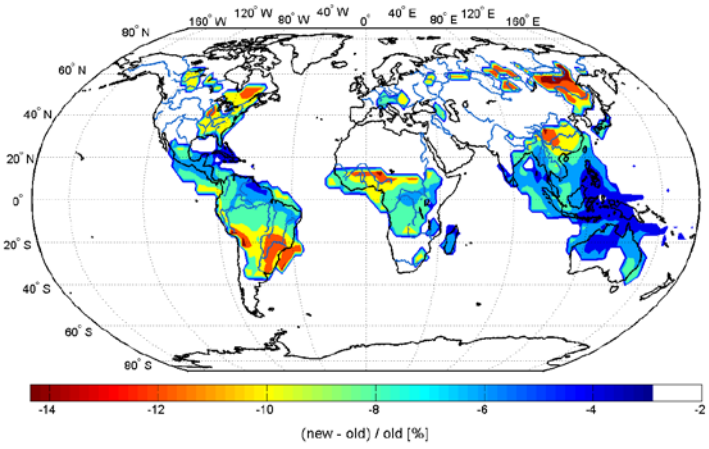

Figure S7: Change in wet deposition fluxes for all deposited species.

Figure S8 depicts global annual changes in dry and wet deposition fluxes for all deposited oVOCs in the present modeling study. The largest increase in dry deposition is observed for MVK, MAC and glyoxal, which were not deposited previously. The largest decrease in wet deposition was observed for the lumped peroxide category ROOH, which is formed from RO_2+HO_2 type reactions (S44).

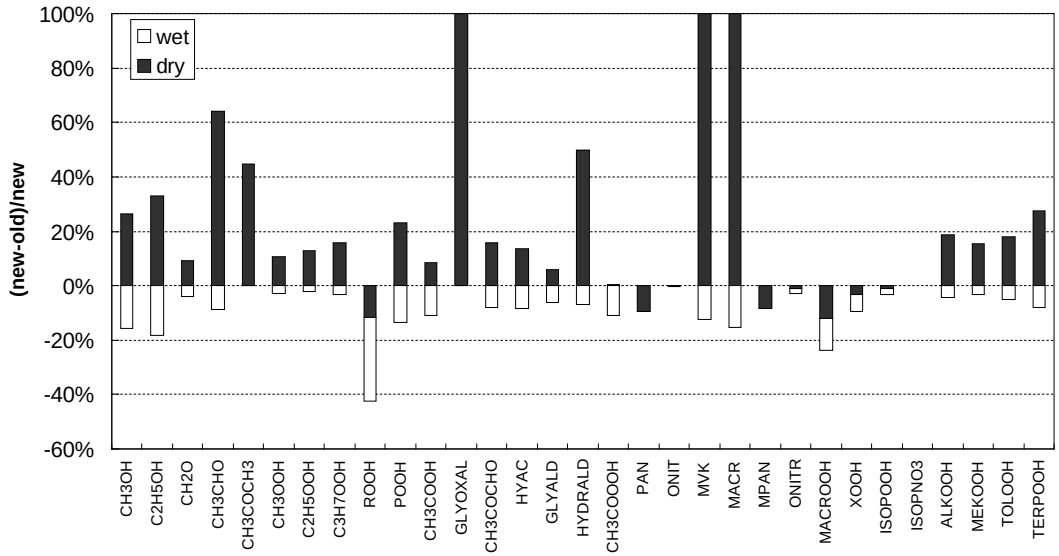

Figure S8: Changes in dry and wet deposition fluxes for all oVOCs deposited in MOZART

6.3. Global gas-phase deposition fluxes

Using the revised deposition scheme we calculate that 37% of the carbon emitted as NMVOC is wet and dry deposited in the gas phase. This likely represents a lower limit because the chemical mechanism used in MOZART-4 is not carbon-conserving. The mechanism was developed relying on the assumption that highly oxidized species, not accounted for by the lumping scheme, would rapidly fall out of the system (e.g. via deposition losses to surface or aerosols) and would therefore not participate in any further gas phase chemistry. While CO_2 produced from oxidization is explicitly included in the mechanism, it is typically not tracked as a species in global model runs. In order to test the effect we run the MOZART-4 mechanism in a 0D box model for a mixture of isoprene, monoterpenes and hydrocarbons, which account for a large fraction of the initial carbon oxidized to oVOC. The mechanism is run as a non-diluting box initialized with different combinations of a mix between 100 ppbv isoprene, 30 ppbv total monoterpenes and 10 ppbv total hydrocarbons (C_2, C_3, C_4 and C_5). OH and ozone are held fixed at 5 x 10^6 molecules/cm^3 and 50 ppbv respectively. NO is varied between 3 and 3000 pptv. Only chemical degradation of the initial NMVOC mix is modeled to investigate the effect of lumping on the carbon budget. Figure S9 plots the total amount of carbon present in the model (including CO_2) relative to the initial amount of carbon as a function of photochemical age (OH x time). For typical conditions encountered in the

planetary boundary layer (green box) we estimate that about 20-30% of the carbon could be lost as a consequence of lumping. If we assume that the 20-30% lost carbon would all have deposited, we would estimate an upper limit of 57-67% deposited.

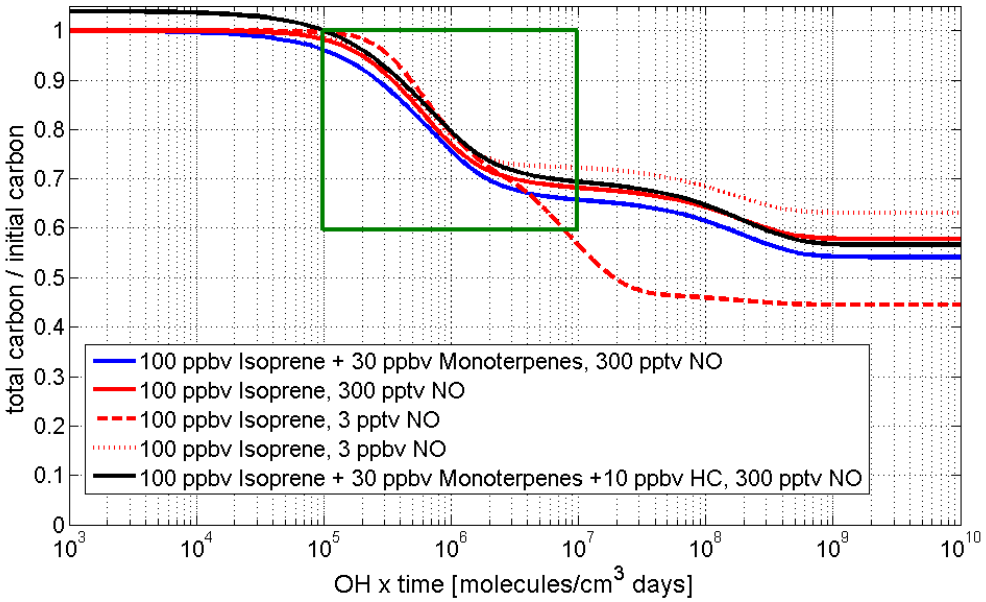

Figure S9: Oxidation of isoprene, monoterpenes and hydrocarbons using the MOZART-4 chemistry mechanism. The green box shows typical conditions encountered in the lower atmosphere.

We can put our results in the context of two recent assessments of the organic carbon budget (S52, S53) recognizing that the amount calculated here likely represents a lower limit. Table S4 summarizes the estimated amount of gas phase deposition relative to the NMVOC emission flux on a carbon basis for three studies. The study by Goldstein and Galbally (S52) acknowledges that neither wet nor dry deposition of gas-phase VOC to terrestrial surfaces has been properly quantified. Their deposition estimates rely on a study by Willey et al. (S53) who assessed the magnitude of global wet deposition based on rain water analysis of dissolved organic matter. Goldstein and Galbally (S52) take a first guess that wet and dry deposition are of similar magnitude (i.e. wet/dry = 1). In our present model runs the ratio between wet and dry deposition changes from 1.22 (control run without inclusion of the fast dry deposition scheme for oVOCs) to 0.87 (sensitivity run with fast dry deposition scheme for oVOCs). This represents a ~40% change in the ratio between wet and dry deposition. Our model runs suggest that the deposition estimate used by Goldstein and Galbally (S52) is likely too low. Compared to their 15% (S52) we estimate 37% as a lower limit. Hallquist et al. (S54) state that vapor deposition is one of the most uncertain terms in constructing global budgets of SOA. Their estimate for vapor deposition is deduced from an indirect assumption that the globally averaged OC/S (organic carbon to sulfur) ratio in particles is about 3:2 (range: 3:1 to 3:4). Taking the sulfur budget as relatively well known they apply the OC/S ratio to estimate a global particulate deposition flux of organic carbon (i.e. 60-240 TgC/a; best estimate: 150 TgC/a). Using a top-down approach (assuming that the primary VOC flux into the atmosphere is well constrained) they subtract the particulate deposition flux from the total

estimated deposition flux (particles plus gases) arriving at a best estimate of 800 TgC/a for gases. This is about 60% relative to the primary NMVOC emission flux. If we assume that the 20-30% of carbon lost by the MOZART-v4 gasphase mechanism would normally be all deposited we calculate an upper limit of 57-67% for the deposition of organic carbon. This also includes particulate organic carbon, which is not explicitly modeled by MOZART-v4. Subtracting the best estimate for the particulate organic carbon deposition flux (11% based on 150 TgC/a; S54) the deposition of vapors estimated here would fall between 46 - 56 %.

Table S4: Comparison of organic vapor deposition relative to the NMVOC emission flux on a carbon basis.

	Mean [TgC/a]	**Comments**
this study	37%	Lower limit
this study	46-56%	Best estimate
this study	57-67%	Upper limit
Goldstein et al.(2007) (S52)	15±7%	Best estimate
Hallquist et al. (2009) (S54)	60%	Best estimate

6.4. Changes in OH, ozone and oVOC

The modifications in dry deposition result in small changes for tropospheric ozone concentrations in the surface, which decrease (by about 3%) throughout the northern hemisphere and increase (by 0.5-1.5 %) above the Amazon, South East Asia and portions of equatorial Africa (Figure S10). OH concentration in the surface layer can increase by up to 15% over land, where the majority of VOCs is released (Figure S11). Figures S10 and S11 show changes for ozone and OH in September. September and October represent the peak of the dry season in the Amazon region, which produces a significant amount of biogenic VOC. Changes during other months are qualitatively comparable, with the lowest differences observed during seasons where vegetation is inactive (e.g. winter in the northern hemisphere). Changes in surface layer concentrations of oVOCs are on the order of 30-60% over land. As typical examples figures S12, S13, S14 and S15 show the relative change of MVK, MAC, CH3OOH and ROOH respectively for October. The most pronounced decreases are observed over densely forested areas. Certain more oxidized oVOCs, such as ROOH, exhibit a significant decrease that extends over large areas including oceans.

Potential consequences for modeling SOA:

Changes of oxygenated VOC (oVOC) concentrations, which act as precursor gases for SOA formation, translate proportionally to concentration changes of more oxidized, semivolatile OC (oSOC) which partition between the gas and particle phase. Assuming OH as the key oxidizing agent and steady state, the change of oVOC can be related to a decreased SOA concentration [K_{OM} x M_0 x oSOC(gas)] according to:

$$oSOC(gas) = \frac{y \cdot k_{oh-oVOC} \cdot oVOC \cdot OH}{k_{oh-oSOC(gas)} \cdot OH + (1 + K_{OM} \cdot M_0)\frac{v_d}{h}}$$, where

$oSOC(particle) = K_{OM} \cdot oSOC(gas) \cdot M_0$, K_{om} represents the partitioning coefficient, M_0 the preexisting aerosol mass, k_{oh} the reaction rates with respect to OH in the gasphase, h the PBL height, v_d the deposition velocity (assuming it is the same for the gas and aerosol fraction) and y the yield from the precursor gas (oVOC). For example as a conservative estimate we can assume that the total aerosol mass stays constant; then the oVOC change translates linearly to the oSOC(particle) change. Under more realistic conditions the SOA mass M_0 will also decrease (e.g. by dilution and associated evaporation if the equilibrium is pulled to the gasphase due to increased depositional losses). This would result in larger decreases.

Dry deposition velocities (v_d) for oSOC in the gasphase are typically modeled according to Wesely (S40), where f_0 is set to 0 (e.g. S55). Using the above mentioned equation we can investigate the impact of underestimated dry deposition velocities for oSOC on their particle concentrations (i.e. looking at the ratio of oSOC(gas) for two different assumptions of v_d). As an example we use conditions representative for the Amazon: Midday R_c for a compound with an HLC of 300 M/atm changes from 131 s/m to 99 s/m (~25%), when f_0 is set to one (instead of zero). Assuming an OH density of ~3e6 molecules/cm3 (e.g. S56), an OH rate constant (for oSOC(gas)) of 2e-12 cm3/s, a PBL height of 1200m, M_0 of 0.5-1 ug/m3 (S57), a K_{om} for oSOC between 0.04-0.17 m^3/ug (based on the low volatility products for b- and a-pinene; S58) and v_d changing from 0.75 to 1 cm/s (~1/R_c), the oSOC concentration would decrease by 5-22% in the aerosol phase. The decrease of a high volatility oSOC (e.g. K_{om} ~ 0.004 m^3/ug; S58) would be about 30%. For comparison it is noted that the lifetime of organic aerosols (burden/source strength) in climate models is typically calculated to be about 4-6 days (S59). For PBL aerosol above tropical regions this would correspond to a deposition velocity of 0.3 cm/s (v_d ~ h/tau, if h=1200m).

Combining the effect of a decrease in the oVOC precursor concentration (i.e. 30-60% based on explicit Mozart model runs) and oSOC gasphase concentration (5-22% and 30% for the low and high volatility products respectively based on the above discussion) can result in a potential change on the order of 36 to 105% for individual SOA species in the surface layer over forested regions.

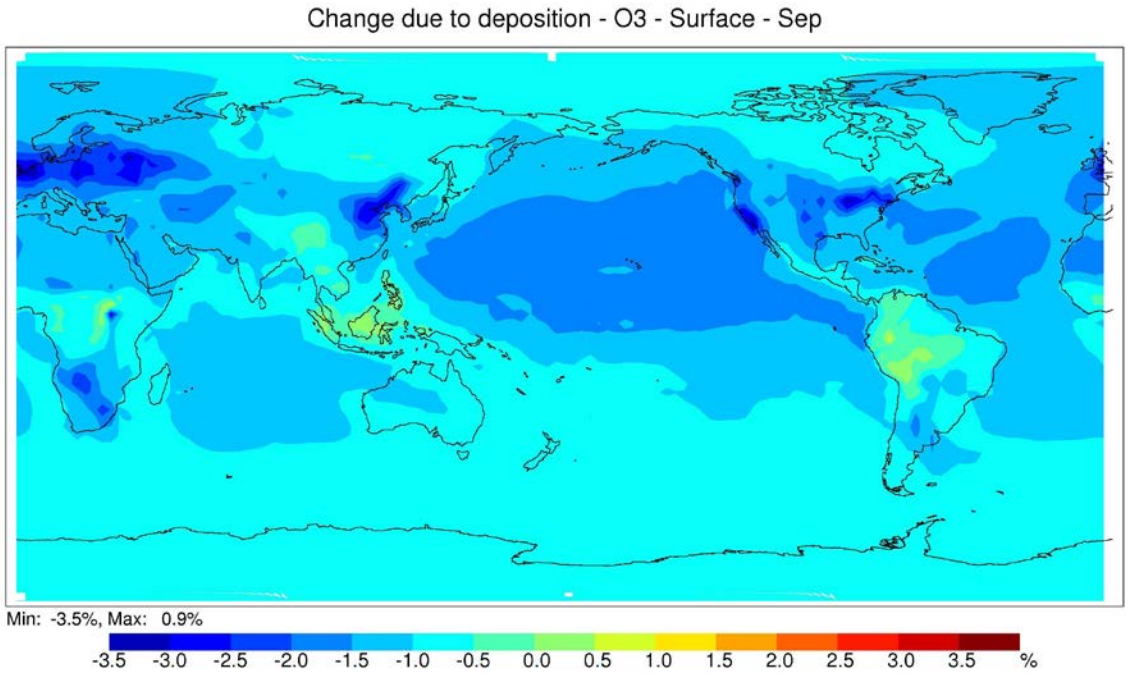

Figure S10: Relative change of surface layer ozone due to increases in dry deposition for September.

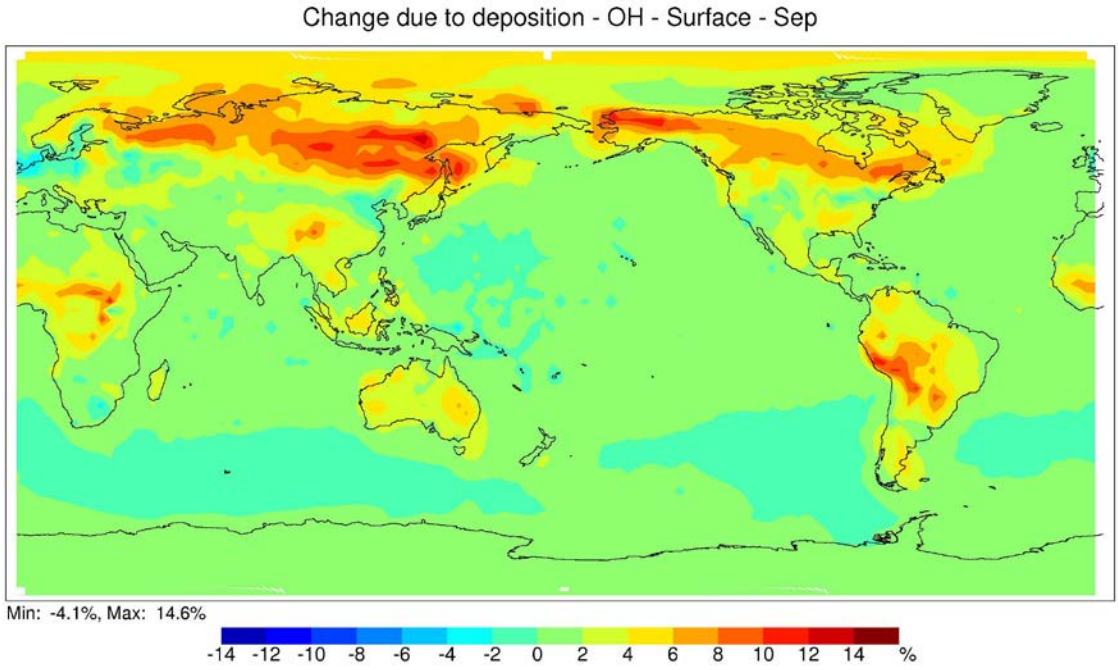

Figure S11: Relative change in surface layer OH due to increases in dry deposition for September.

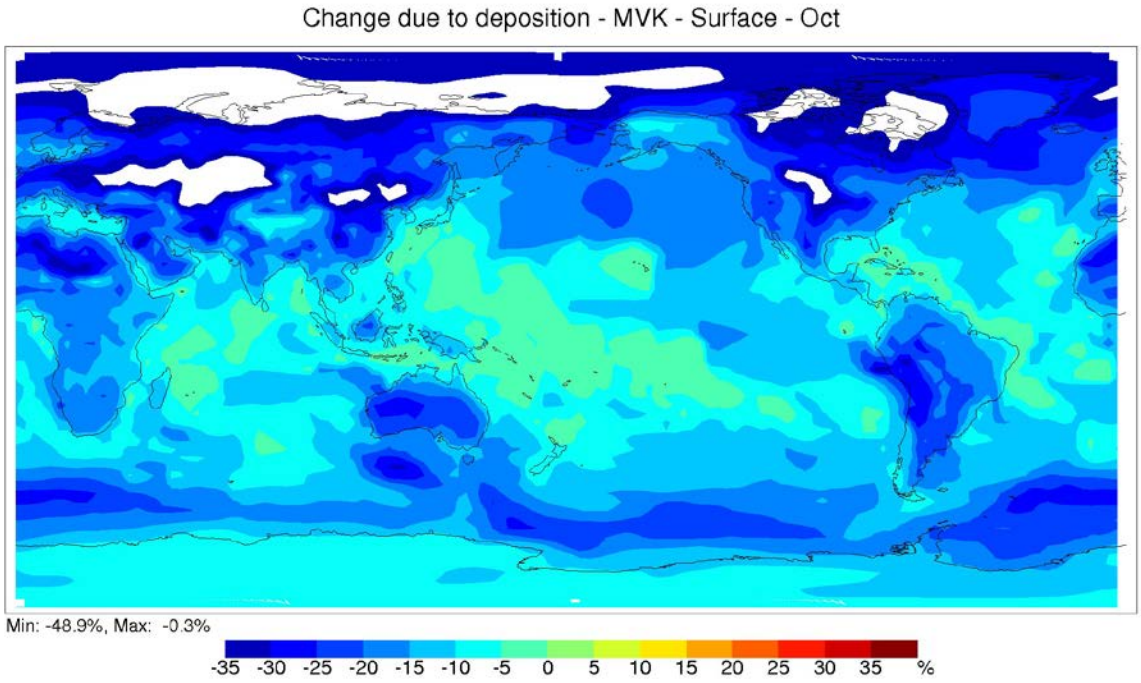

Figure S12: Relative change in surface layer MVK concentrations due to increases in dry deposition for September.

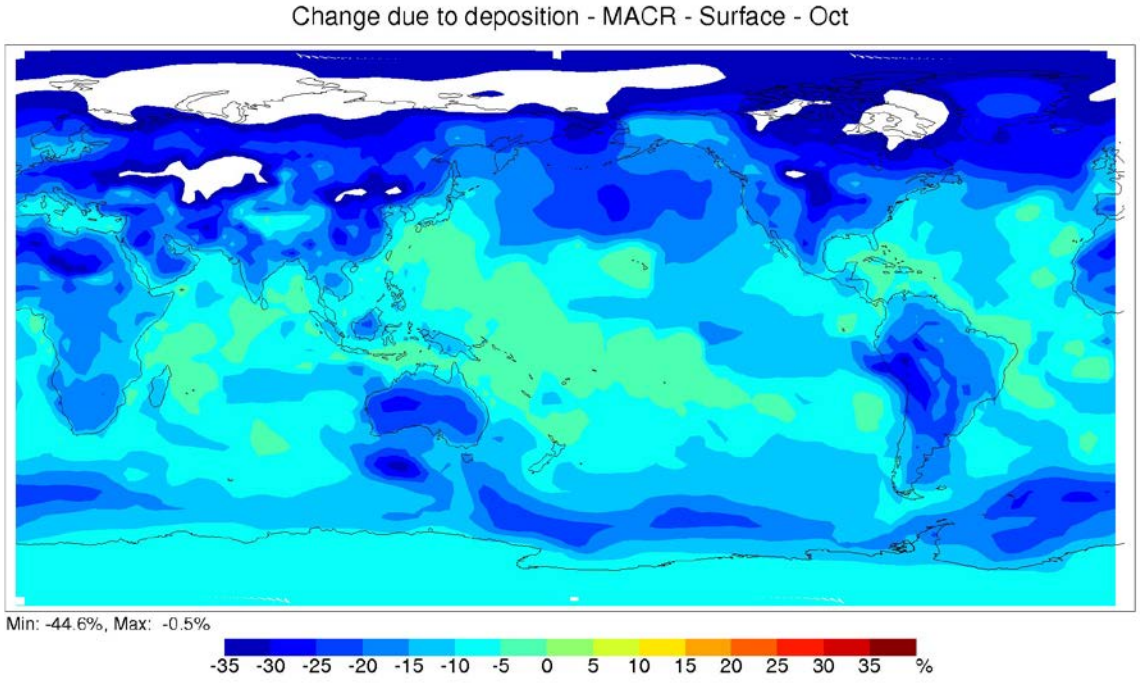

Figure S13: Relative change in surface layer MAC concentrations due to increases in dry deposition for September.

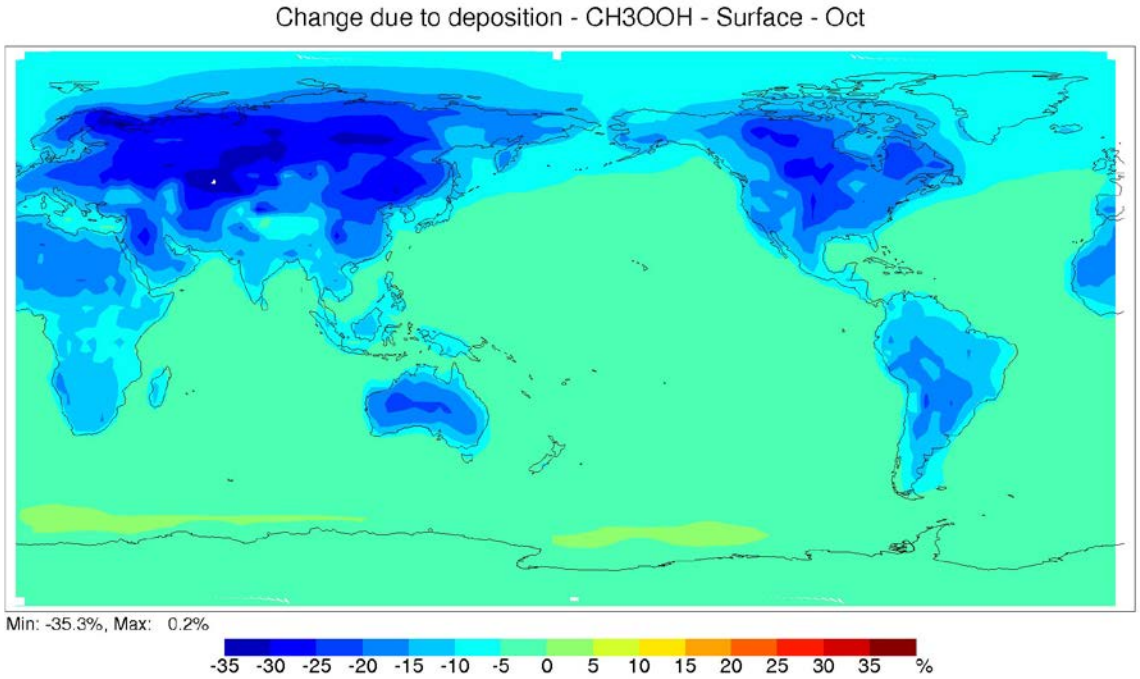

Figure S14: Relative change in surface layer CH3OOH concentrations due to increases in dry deposition for September.

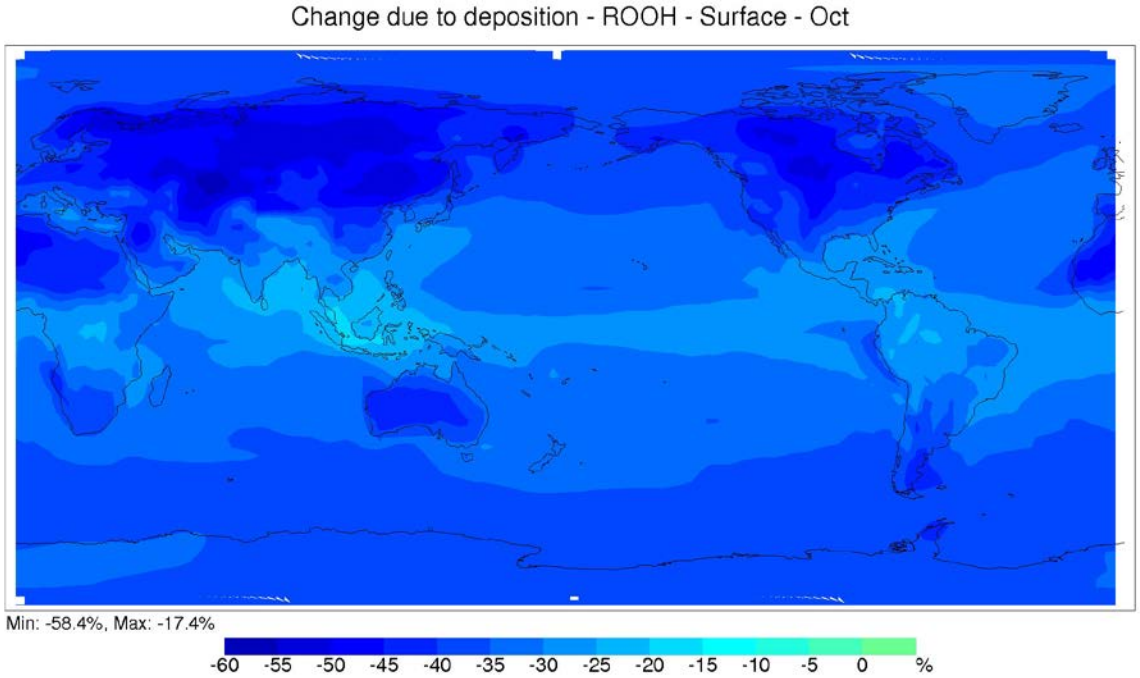

Figure S15: Relative change in surface layer ROOH concentrations due to increases in dry deposition for September.

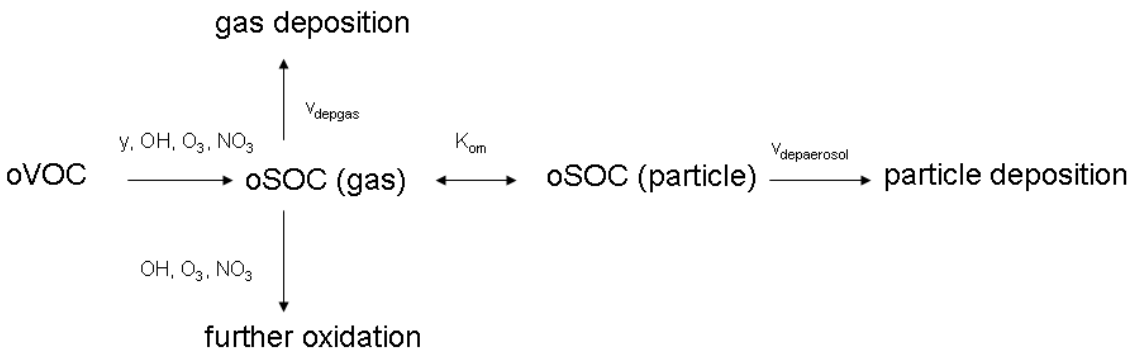

Figure S16: Schematic picture of oVOC oxidation and SOA partitioning. oVOC: volatile oVOC precursor, oSOC: oxidized semivolatile organic compound in gas and particle phase; y: yield of oSOC; K_{om}: partition coefficient; vdepgas, vdepaerosol: deposition velocity for gas and particle phase.

References

S1. D.B. Clark and D. A. Clark, *For. Ecol. Manage.* **137**, 185 (2000).

S2. G. Katul et al., *Boundary-Layer Meteorology* **93**, 1 (1999).

S3. R. Yokelson et al., *Atmos. Chem. Phys.* **7**, 5175 (2007).

S4. M.A.Carroll et al., *J. Geophys. Res* **106** , 24275 (2001).

S5. S. Martin et. al., *Reviews of Geophysics*, 48, in press (2010).

S6. W. Lindinger et al., *Chem. Soc. Rev.* **27**, 347 (1998).

S7. A. Hansel et al., *Rapid Commun. Mass Spectrom.* **12**, 871 (1998).

S8. J. de Gouw and C. Warneke, *Mass Spectrom. Rev.* **26**, 223 (2007).

S9. A. Wisthaler et al., *Atmos. Environm.* **35**, 6181 (2001).

S10. N. Schoon et al., *International Journal of Mass Spectrometry* **239**, 7 (2004).

S11. J. Greenberg et al., *J. Chromatogr.* **676**, 389 (1994).

S12. S. von Caemmerer and G.D. Farquhar, *Planta* **153**, 376 (1981).

S13. A. Castagna and A. Ranieri, *Environmental Pollution* **157**, 1461 (2009).

S14. S. Rozen and H.J. Skaletsky: Primer3 on the WWW for general users and for biologist programmers. In: Krawetz S, Misener S (eds) Bioinformatics Methods and Protocols: Methods in Molecular Biology. Humana Press, Totowa, NJ, 365 (2000).

S15. A. Brunner et al., *BMC Plant Biology*, **4**/**14**, doi:10.1186/1471-2229-4-14 (2004).

S16. A.L. Bookout and D. J. Mangelsdorf, *Nuclear Receptor Signaling*, **1**, e012. doi: 10.1621/nrs.01012 (2003).

S17. E. Alméras et al., *The Plant Journal* **34**, 205 (2003).

S18. S. Pasqualini et al., *New Phytologist* **181**, 860 (2008).

S19. M. Rizzo et al., *Journal of Plant Physiology* **164**, 945 (2006).

S20. R. Sunkar, *Plant J.* **35**, 452 (2003).

S21. S.M. Rodrigues et al., *J. Exp. Bot.* **57**, 1909 (2006).

S22. C. Santos et al., *Plant Physiology* **138**, 909, (2005).

S23. M.L. Wesely and R.L. Hart: Variability of short term eddy-covariance estimates of mass exchange, in: The forest atmosphere interactions, (eds) Hutchison, B. and Hicks,B., D. Reidel publishing Company, Dortrecht, The Netherlands, 591 (1985).

S24. W.F. Dabberdt et al., *Science* **260**, 1472 (1993).

S25. M.R. Raupach, *Agric. For. Meteorol.* **47**, 85 (1986).

S26. E. Nemitz et al., *Agric. For. Meteorol.* **105**, 385 (2000).

S27. T. Karl et al., *J. Geophys. Res.* **109**, D18306, doi:10.1029/2004JD004738 (2004).

S28. T. Karl et al., *J. Geophys. Res.* **106**, 24157 (2001).

S29. T. Karl et al., *Atmos. Chem. Phys.* **2**, 279 (2002).

S30. H.J.I. Rinne et al., *Geophys. Res. Lett.* **28**, 3139 (2001).

S31. J. Lelieveld et al., Nature **452**, 737 (2008).

S32. C. Stroud et al., *J. Geophys. Res*. **110**, D17303, doi:10.1029/2005JD005775 (2005).

S33. C.A. Paulson, *J. Appl. Meteor.* **9**, 857 (1970).

S34. A. Guenther et al., *Atmos. Chem. Phys.* **6**, 3181 (2006).

S35. A. Guenther et al., *J. Geophys. Res.* **100**, 8873 (1995).

S36. D.D. Baldocchi et al., *Atmos. Environ.* **21**, 91 (1987).

S37. C.J.T. Spitters et al., *Agri. Forest. Meterology* **38**, 217 (1986).

S38. M. Goudriaan, and H.H. van Laar, Modelling potential crop growth processes, in: Current issues in production ecology (Kluwer Academic Publishers, 1994).

S39. R. Leuning et al., *Plant, Cell & Environment* **18**, 1183 (1995).

S40. M.L.Wesely, *Atmos. Environ.* **23**, 1293 (1989).

S41. L. Zhang et al., *Atmos. Environ.* **36**, 537 (2002).

S42. A. Tani and N. Hewitt, *Environ. Sci. Technl.*,**43** ,8338 (2009).

S43. G.A. Alexandrov and Y. Yamagata, *Ecological Modeling* **200**, 189 (2007).

S44. L.K. Emmons et al., *Geosci. Model Dev.* **3**, 43 (2010).

S45. J. Walmsley and M. Wesely, *Atmos. Environ,* **30**, 1181 (1996).

S46. M. Wesely and B. Hicks, *Atmos. Environ,* **34**, 2261 (2000).

S47. G. Bonan et al., *Glob. Change Biology* **9**, 1543 (2003).

S48. M. Sanderson et al., *J. Atmos. Chem.* **46**, 15 (2003).

S49. T. Teklemariam and J.P. Sparks, *Plant Cell Envrion,* **27**, 1149 (2004).

S50. J.P. Sparks et al., *Geophys. Res. Lett,* **30**, doi: 10.1029/2003GL018578 (2003).

S51. G.P. Brasseur et al., *J. Geophys. Res.* **103**, 28265 (1998).

S52. A.H. Goldstein and I. Galbally I, *Environ. Sci. Technol.* **41**, 1515 (2007).

S53. J.D. Willey, Kieber, R.J., Eyman, M.S., and G.B Avery, *Global Biogeochemical Cycles,* **14**, 139 (2000).

S54. M. Hallquist et al., *Atmos. Chem. Phys.* **9**, 5155 (2009).

S55 S.H. Chung and J.H. Seinfeld, *J. Geophys. Res.* **107**, DOI: 10.1029/2001JD001397 (2002).

S56 T. Karl et al. *J. Geophys. Res.* **112**, DOI: 10.1029/2007JD008539 (2007).

S57 Q. Chen et al., *Geophys. Res. Lett.* **36**, DOI: 10.1029/2009GL039880 (2010).

S58 R.J. Griffin et al., *J. Geophys. Res.* **104**, 3555 (1999).

S59. P. Stier et al., *J. Climate,* **19**, 3845 (2006).